Coty, W. A., Schrader, W. T., & O'Malley, B. W. (1979) *J. Steroid Biochem. 10*, 1.
Jaffe, R. C., Socher, S. H., & O'Malley, B. W. (1975) *Biochim. Biophys. Acta 399*, 403.
Kuhn, R. W., Schrader, W. T., & O'Malley, B. W. (1975) *J. Biol. Chem. 250*, 4220.
Kuhn, R. W., Schrader, W. T., Coty, W. A., Conn, P. M., & O'Malley, B. W. (1977) *J. Biol. Chem. 252*, 308.
O'Malley, B. W., Toft, D. O., & Sherman, M. R. (1971) *J. Biol. Chem. 246*, 1117.
O'Malley, B. W., Vedeckis, W. V., Birnbaumer, M. E., & Schrader, W. T. (1977) in *Molecular Endocrinology* (MacIntyre, I., & Szelke, M., Eds.) p 135, Elsevier/North-Holland Biomedical Press, Amsterdam.
Puca, G. A., Nola, E., Sica, V., & Bresciani, F. (1972) *Biochemistry 11*, 4157.
Puca, G. A., Nola, E., Sica, V., & Bresciani, F. (1977) *J. Biol. Chem. 252*, 1358.
Schrader, W. T. (1975) *Methods Enzymol. 36*, 187.
Schrader, W. T., Toft, D. O., & O'Malley, B. W. (1972) *J. Biol. Chem. 247*, 2401.
Schrader, W. T., Heuer, S. S., & O'Malley, B. W. (1975) *Biol. Reprod. 12*, 134.
Schrader, W. T., Kuhn, R. W., & O'Malley, B. W. (1977a) *J. Biol. Chem. 252*, 299.
Schrader, W. T., Coty, W. A., Smith, R. G., & O'Malley, B. W. (1977b) *Ann. N.Y. Acad. Sci. 286*, 64.
Sherman, M. R., & Diaz, S. C. (1977) *Ann. N.Y. Acad. Sci. 286*, 81.
Sherman, M. R., Atienza, S. B. P., Shansky, J. R., & Hoffman, L. M. (1974) *J. Biol. Chem. 249*, 5351.
Sherman, M. R., Tuazon, F. B., Diaz, S. C., & Miller, L. K. (1976) *Biochemistry 15*, 980.
Sherman, M. R., Pickering, L. A., Rollwagen, F. M., & Miller, L. K. (1978) *Fed. Proc., Fed. Am. Soc. Exp. Biol. 37*, 167.
Sica, V., Nola, E., Puca, G. A., & Bresciani, F. (1976) *Biochemistry 15*, 1915.
Vedeckis, W. V., Schrader, W. T., & O'Malley, B. W. (1978) in *Biochemical Actions of Hormones* (Litwack, G., Ed.) p 321, Academic Press, New York.
Vedeckis, W. V., Schrader, W. T., & O'Malley, B. W. (1979) in *Steroid Hormone Receptor Systems* (Leavitt, W. W., & Clark, J. H., Eds.) p 309, Plenum Press, New York.
Vedeckis, W. V., Freeman, M. R., Schrader, W. T., & O'Malley, B. W. (1980) *Biochemistry* (preceding paper in this issue).
Walsh, K. A. (1975) in *Proteases and Biological Control*, p 1, Cold Spring Harbor Laboratory, Cold Spring Harbor, NY.
Wrange, Ö., & Gustaffson, J.-Å. (1978) *J. Biol. Chem. 253*, 856.

Raman Scattering in Bilayers of Saturated Phosphatidylcholines. Experiment and Theory†

David A. Pink,* Trevor J. Green, and Dennis Chapman

ABSTRACT: Raman spectroscopy has been applied to a model biomembrane structure in order to obtain information about phospholipid hydrocarbon chain ordering. The intensity of the 1130-cm^{-1} Raman line obtained from a dipalmitoylphosphatidylcholine (DPPC) coarse aqueous dispersion has been measured as a function of temperature. The intensities of this line and a reference line were taken as peak areas. The main phase transition together with the pretransition was observed. A theory of chain conformations as a function of temperature and rules for the assignment of Raman scattering intensities for this line have been constructed. Good agreement with the DPPC experimental data has been obtained. Predictions for the intensity of this line as a function of temperature from dimyristoyl- and distearoylphosphatidylcholine dispersions have also been made.

Information about hydrocarbon chain order and mobility in model biomembrane structures is of importance in understanding the perturbation which intrinsic molecules such as cholesterol or proteins can produce when present within the lipid bilayer. Recent studies using the physical techniques electron spin resonance and deuterium nuclear magnetic resonance spectroscopy give contradictory answers (unless time-scale arguments are used) to the question of whether intrinsic proteins cause either an ordering or an immobilization of adjacent lipids or, alternatively, a disordering and fairly rapid exchange between lipid environments [see Chapman et al. (1979) for a recent review].

It is thus useful to examine these perturbation effects with a probeless technique which operates on a very rapid time scale compared to magnetic resonance experiments. In principle Raman spectroscopy should provide additional information on lipid hydrocarbon chain ordering, although previously there have been differing approaches to the quantitative interpretation of experimental data.

The technique of Raman spectroscopy has found use in the study of lipids in both model and biological membranes. Several workers have made use of the temperature dependence

† From the Institut für Neurobiologie der Kernforschungsanlage, D-517 Jülich, Federal Republic of Germany (D.A.P), and the Department of Biochemistry and Chemistry, Royal Free Hospital School of Medicine, University of London, 8 Hunter Street, London WC1N 1BP, England (T.J.G. and D.C.). *Received June 11, 1979; revised manuscript received September 10, 1979.* This work was supported in part by the National Science and Engineering Research Council of Canada, the Science Research Council and the Wellcome Trust.

* Permanent address and author to whom correspondence should be addressed: Theoretical Physics Institute, St. Francis Xavier University, Antigonish, Nova Scotia B2G 1C0, Canada.

0006-2960/80/0419-0349$01.00/0

of the Raman spectrum of phospholipid dispersions in order to examine the effects of membrane components [e.g., cholesterol (Lippert & Peticolas, 1971), polypeptides (Chapman et al., 1977), and proteins (Curatolo et al., 1978)] on the lipid hydrocarbon chain order.

In particular, line intensities in the 1100-cm^{-1} region of the Raman spectrum of a dipalmitoylphosphatidylcholine (DPPC) aqueous dispersion reveal abrupt changes as the bilayers undergo the gel–liquid crystal transition at 41 °C (Lippert & Peticolas, 1971; Gaber & Peticolas, 1977; Yellin & Levin, 1977b; Gaber et al., 1978a). At temperatures below this transition temperature (T_c), the main spectral features in this region are the 1130- and 1064-cm^{-1} lines, caused by skeletal optical ($k = 0$) mode vibrations of the hydrocarbon chains (Snyder, 1967; Tasumi et al., 1962; Lin & Koenig, 1962), and a broad 1100-cm^{-1} line which has also been assigned to a vibrational mode of the hydrocarbon chain (Spiker & Levin, 1975; Gaber et al., 1978a) with a small intensity contribution from a stretching mode of the lipid phosphate group (Spiker & Levin, 1975; Gaber et al., 1978b). As the lipid temperature is raised through T_c, the 1130-, 1064-, and 1100-cm^{-1} lines reduce in intensity, while a broad band having maximum intensity at 1090 cm^{-1} appears; this latter band is considered to arise from gauche rotations in the hydrocarbon chains (Lippert & Peticolas, 1971; Gaber et al., 1978a; Snyder, 1967).

It is of interest to interpret these spectral changes in terms of conformational changes in the lipid hydrocarbon chains. The characteristic drop in intensity of the DPPC 1130-cm^{-1} line at T_c was attributed by Lippert & Peticolas (1971) to the cooperative change of the palmitic chains from the all-trans to a fluid state. As discussed by Marsh (1974), lipid hydrocarbon chain fluidity is associated with rotational isomerisms of C–C single bonds, there being two gauche conformations ($g^{\pm}$) having intrachain or internal energy E_g relative to the trans conformation (t). At a given temperature steric hindrance within the lipid bilayer imposes restrictions on possible rotational permutations along each chain, certain types of chain conformation (e.g., "kinks") being more probable due to their favorable packing characteristics. Marsh (1974) interpreted the data of Lippert & Peticolas (1971) by assuming that only those hydrocarbon chains in the all-trans conformation undergo the 1130-cm^{-1} skeletal optical mode vibration and thus give rise to the 1130-cm^{-1} Raman line. However, hydrocarbon chains containing gauche bonds may also contribute to the intensity of this line (Snyder, 1967). Gaber & Peticolas (1977) assumed that each trans C–C bond, in a sequence of at least three, makes a constant intensity contribution to the 1130-cm^{-1} line; thus, they indicated that the line intensity was a function of both the number and arrangement of trans bonds within the hydrocarbon chains. Such a situation does not allow trans and gauche bond content or chain conformations to be determined unequivocally from 1130-cm^{-1} line relative intensity measurements.

Besides the abrupt reduction in intensity of the 1130-cm^{-1} line at T_c, there are a gradual decrease in its intensity with respect to reference lines in the Raman spectrum as the DPPC bilayer temperature approaches T_c (Gaber & Peticolas, 1977; Yellin & Levin, 1977a–c; Gaber et al., 1978a) and a sharp but small loss approximately 7 °C below T_c (Gaber & Peticolas, 1977; Yellin & Levin, 1977b; Gaber et al., 1978a) attributed to the pretransition or premelting event which has been observed by using differential scanning calorimetry (Chapman et al., 1967). It may therefore be concluded that conformations other than the all-trans state occur in the hydrocarbon chains at low temperatures.

In this paper we present measurements of the 1130-cm^{-1} line intensity as a function of temperature, obtained from a DPPC coarse aqueous dispersion, and describe a theory of the intensity of this line which is applicable to similar saturated lipids (we predict the corresponding intensities from dimyristoylphosphatidylcholine, DMPC, and distearoylphosphatidylcholine, DSPC). The theory is in two parts: in the first part we outline a dynamical model described in greater detail elsewhere (Caillé et al., 1980) which involves the consideration of the detailed conformations of the hydrocarbon chains; in the second part we assign Raman intensities at 1130 cm^{-1} to each state of the chain. We comment on the theories of Marsh (1974) and Gaber & Peticolas (1977) and on some of the conclusions of Yellin & Levin (1977a,b) concerning attempts at quantitative analyses of lipid hydrocarbon chain properties using Raman spectroscopic data.

Theory

A model for the conformer dynamics of a saturated hydrocarbon chain in a lipid bilayer is described elsewhere (Caillé et al., 1980) where it was used to understand the chain-length dependence of transition temperatures and enthalpies in phosphatidylcholines and the diffusion rate of Na^+ ions through the walls of DPPC vesicles and to successfully reproduce the slightly asymmetric phase diagram of a mixture of DPPC and DMPC. One application of a simplified version of the model was the calculation of the dependence of transition enthalpy upon cholesterol concentration in DPPC–cholesterol mixtures (Pink & Carroll, 1978; Pink & Chapman, 1979), the results agreeing with those of Estep et al. (1978). We therefore feel moderately confident in using it to calculate Raman intensities for hydrocarbon chains.

The model assumes that each site of a triangular lattice is occupied by a hydrocarbon chain containing M carbon nuclei and denoted by C-M, which may be in any of the following states. (1) The first is the all-trans ground state of internal energy 0 and area A_G, labeled G. (2) The second are a number of intermediate energy states which, because they have an effective area not much larger than A_G, can be excited significantly below the main transition temperature $T_c(M)$. The number of these states is proportional to M, and they are labeled 1, 2, ..., k. The third is one high-energy "melted" state which represents all the states omitted above. It is labeled E, has an area A_E, a degeneracy $D_E(M) \propto 3^M$, and an internal energy E_E. Internal energy refers to that needed to excite the given state of a chain isolated from other chains. The areas in question are defined as $A_n = A_G L_G / L_n$, where L_G is the length of the all-trans state and A_n and L_n are the area and length of the state labeled n. This definition assumes that the density does not change significantly on melting, and, in fact, the change is ~4% (Nagle, 1973a). The length is measured from the carbonyl group to the terminal methyl group and is the projection of the chain onto a normal to the bilayer. The length of an all-trans C-M chain is proportional to $M - 1$. We shall simplify the chain by assuming that the bond angle is 120° and shall consider only those kinklike states wherein the chain remains in a plane perpendicular to the bilayer plane, i.e., $...g,t^{\pm},g...g,t^{\mp},g...$, as intermediate states (see Figure 1). Rotations about the first two bonds are not allowed in intermediate states.

We take the view that interactions between the polar head groups and between them and water keep the bilayer in existence, and these provide an effective lateral pressure acting on the hydrocarbon chains, due to the presence of the other chains (Marcelja, 1974). A pressure–area term thus plays the part of interchain steric repulsion and is probably satisfactory

Table I: C-M Hydrocarbon Chain State Configurations and Relative Raman Intensities

state		length (C–C bond units)	degeneracy	rel Raman intensity (C-M) C-14	C-16	C-18	internal energy
all-trans	G	$M-1$	1	196.0	256.0	324.0	0
intermediate	1	$M-2$	4	82.0	122.0	170.0	
	2	$M-3$	4	26.0	50.0	82.0	E_g
	3	$M-4$	4	2.0	10.0	26.0	
	4 kink	$M-2$	$2M-12$	100.0	144.0	196.0	
	5	$M-3$	$2M-16$	36.0	64.0	100.0	$2E_g$
	6	$M-4$	$2M-20$	4.0	16.0	36.0	
	7	$M-3$	$8M-64$	26.83	50.88	82.9	
	8	$M-4$	$16M-160$	2.25	10.5	25.5	$3E_g$
melted	E	$20.4(M-1)/34.0$	$D_E(M)$	10	15	20	$E_E(M)$

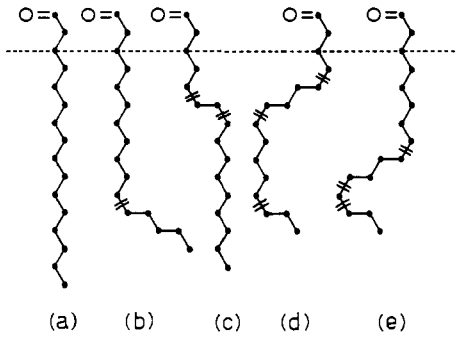

FIGURE 1: The all-trans state and some intermediate states for a C-16 chain. Double slashes indicate bonds around which a gauche rotation has occurred. The internal energies (E), lengths (L), areas (A), and degeneracies (D) are as follows: (a) $E = 0$, $L = 15$, $A = 20.4$ Å^2, and $D = 1$; (b) $E = E_g$, $L = 13$, $A = 23.54$ Å^2, and $D = 2$; (c) kink, $E = 2E_g$, $L = 14$, $A = 21.86$ Å^2, and $D = 2$; (d) $E = 3E_g$, $L = 12$, $A = 25.5$ Å^2, and $D = 4$; (e) $E = 3E_g$, $L = 12$, $A = 25.5$ Å^2, and $D = 2$. Intermediate states do not have gauche rotations around the two bonds above the dashed line.

for temperatures above $T_c(M)$ but not obviously so for chains with large areas below $T_c(M)$, where there is close packing. The energy of a particular chain depends upon its internal energy, its conformation, and the details of the conformations of its surrounding chains, and it is the last contribution which includes the repulsive steric effects and which we approximate by our interaction Hamiltonian and the pressure–area terms. Below $T_c(M)$, we consider that some configurations must simply be omitted (i.e., assigned an infinite steric repulsive energy) because our averaged interactions probably result in an underestimate of the energy needed to excite such states. Thus, we consider it unlikely for a chain to adopt a large-area configuration of low internal energy with a statistical probability determined only by the internal energy, the effective pressure, and the effective interaction that we shall use. Accordingly, the intermediate states which can be excited significantly below $T_c(M)$ will be selected as those with internal energy $\leq 3E_g$, where E_g is the internal energy needed to form a single gauche bond, and with chain length $\geq M-4$ (in units of the length of a C–C bond of an all-trans chain projected onto the bilayer normal). For $A_G = 20.4$ Å^2 (Tardieu et al., 1973), a DPPC chain in an excited state with length proportional to $M-4$ has an area of 25.5 Å^2. The area of the highly excited melted state was taken as $A_E = 34$ Å^2. The states considered are listed in Table I and, by restriction of the interchain interaction to nearest-neighbor chains, the Hamiltonian is

$$H = \frac{-J_0^M}{2}\sum_{\langle ij\rangle}\sum_{nm} I_{nm}(\Delta_{nm})L_{ni}L_{mj} + \sum_i\sum_n(\Pi A_n + E_n)L_{ni} \quad (1)$$

where J_0^M is the energy of interaction between two parallel all-trans C-M chains and L_{ni} is a lipid chain projection operator for lattice site i and lipid chain state n with n = G, 1, 2, ..., 8, E. $\langle ij\rangle$ represents a sum over nearest-neighbor sites and Δ_{nm} is the distance between two chains in states n and m at sites i and j. Π is the effective lateral pressure and E_n is the internal energy, due to the formation of gauche bonds, of a chain in state n. The energy E_E was plausibly shown to be proportional to M elsewhere (Caillé et al., 1980). The interaction energy is defined, following Wulf (1977), to be

$$I_{nm}(\Delta_{nm}) = \sum_{pq}\frac{S_{np}S_{mq}}{S_0^2}f(\Delta_{nm}) \quad (2)$$

$$S_{np} = 3/2\cos^2\theta_{np} - 1/2 \qquad S_0 = \sum_p S_{Gp}$$

$$f(\Delta_{nm}) = (\Delta_0/\Delta_{nm})^5$$

where $f(\Delta_{nm})$ describes how the interaction changes as the chains separate without changing their conformations, S_{np} is the order parameter of the pth C–C bond when a chain is in its nth state, and θ_{np} is the angle that this bond makes with the normal to the bilayer. We took the radius of an effective cylinder occupied by a chain in state n to be $r_n = (A_n/\pi)^{1/2}$, so that $\Delta_{nm} = r_n + r_m$, and with $\Delta_0 = 2r_G$ the approximation

$$f(\Delta_{nm}) \simeq r_G^5/(r_n r_m)^{5/2} \quad (3)$$

is valid to within a few percent for nearly all states. This approximation is useful when we calculate thermodynamic quantities. Elsewhere (Caillé et al., 1980) it is shown that the degeneracy of the excited melted state is given satisfactorily by $D_E(M) \simeq 6(3)^{M-6}$, and we have used this value here.

The value of E_g lies between 0.35×10^{-13} and 0.55×10^{-13} erg [500–800 cal/mol; Flory (1969)], and we have chosen an average of $E_g = 0.45 \times 10^{-13}$ erg. $J_0^M \propto M$ (Salem, 1962) so that, if any two are determined, then all J_0^M values are obtained. Similarly, $E_E(M) \propto M$ (Caillé et al., 1980) and the determination of one yields the others. J_0^{14}, J_0^{16}, and $E_E(16)$ were determined by fitting to $T_c(14)$, $T_c(16)$, and the heat of transition for C-16, $\Delta H(16)$. We chose $\Pi = 30$ dyn/cm and found that $J_0^{16} = 0.734 \times 10^{-13}$ erg. A reasonable fit for $T_c(12)$ to $T_c(22)$ and for $\Delta H(12)$ to $\Delta H(22)$ was obtained.

In order to calculate the Raman scattering intensity at any temperature relative to the intensity at sufficiently low temperatures when all chains are in their all-trans conformations, we must know how to calculate the intensity of any conformation relative to that of the all-trans state. We shall confine ourselves entirely to consideration of the 1130-cm^{-1} line because detailed calculations have been done on the normal modes of some configurations which contribute to this mode (Snyder, 1967). A normal mode calculation should be performed for the entire lipid molecule, but we consider that such an undertaking is beyond the scope of this work. We shall assume that the 1130-cm^{-1} mode of a chain is sufficiently

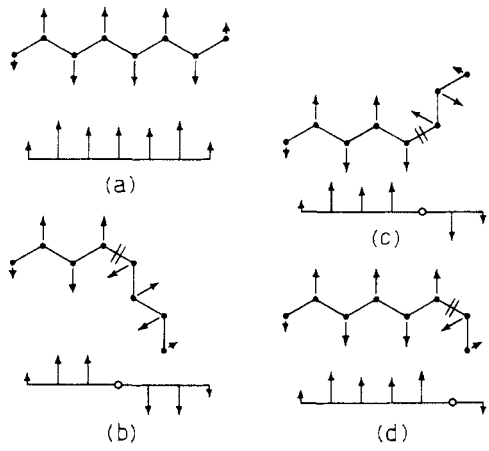

FIGURE 2: Schematic representation of the TO CH_2 motions and normal modes for $CH_3(CH_2)_6CH_3$ in the all-trans state (a) and with one gauche bond (b–d), adapted from Snyder (1967). The motion of other CH_2 groups are deduced from these results. Note the phase change of π across the gauche bond (indicated by a double slash).

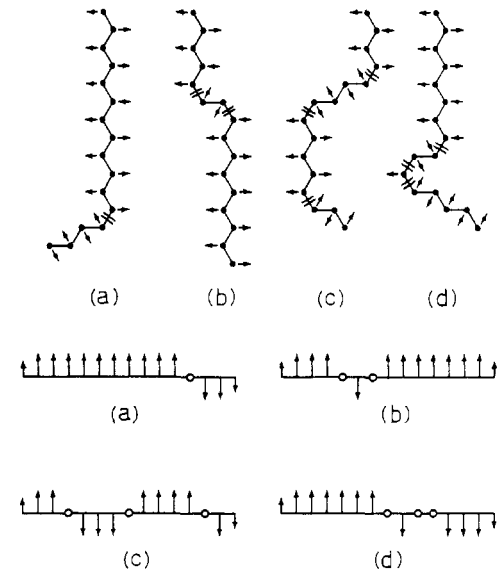

FIGURE 3: Assumed motion of CH_2 groups for a C-16 chain excited in its TO mode, based on an extension of the results of Snyder (1967). The chain has up to three gauche bonds. The assumed normal modes are shown below. In comparison with Figure 2, (a), (b), and (c) are probably correct, but there may be doubt about (d). Note the change in phase of π across each gauche bond (indicated by double slashes).

decoupled from the remainder of the molecule and that our reference mode, the C–N stretching mode, is temperature independent (Gaber & Peticolas, 1977; Gaber et al., 1978a).

Model calculations have been performed on the vibrational modes of infinite polymethylene chains and *n*-paraffins in their all-trans configurations by Tasumi et al. (1962), who used a modified Urey–Bradley force field, by Snyder (1967), who used a valence force field, and by Lin & Koenig (1962). Among many other results they identify a C–C skeletal stretch mode and, if ϕ represents the wave vector in the first Brillouin zone, then at $\phi = 0$ this mode is a transverse optic (TO) mode of A_g symmetry, in which successive CH_2 groups move in opposite directions (Figure 2). It has been assigned a wavenumber of 1142–1143 (Tasumi et al., 1962) and 1061 cm^{-1} [Lin & Koenig (1962), incorrectly we consider]. Snyder (1967) calculated the corresponding wavenumbers for $CH_3(CH_2)_{M-2}CH_3$ and found them to be (units of cm^{-1}) as follows: $M = 6$, 1143; $M = 7$, 1142; $M = 8$, 1141; $M = 14$, 1139; $M = 22$, 1136 [estimated from Figure 8 of Snyder & Schachtschneider (1963)]. Thus, for M sufficiently large ($M \gtrsim 8$) the change in wavenumber with M is smaller than the experimental width of the 1130-cm^{-1} line. It might be noted that the TO skeletal mode apparently mixes with a longitudinal acoustic (LA) mode, associated with in-plane skeletal deformation, at $\phi \approx 0.4\pi$ so that at $\phi = \pi$ the TO mode has become an LA-type in-plane skeletal stretch mode. Both Tasumi et al. (1962) and Snyder (1967) associate this with the observed 1064-cm^{-1} mode, though Lin & Koenig (1962) associate it with the 1130-cm^{-1} mode. We consider that the 1130-cm^{-1} mode has been correctly assigned and described by Snyder (1967).

Snyder (1967) has also calculated the wavenumbers and normal coordinates of various *n*-paraffins with a single gauche bond. Some examples of these are shown in Snyder's Figures 20 and 21 and two points seem clear. (1) For $CH_3(CH_2)_{M-2}CH_3$ with a single gauche bond anywhere in the group, the wavenumber of the TO mode at $\phi = 0$ changes by not more than 5 cm^{-1} for $M = 6$, 7, and 8, and for $M = 14$ with a gauche bond in the center of the group, which is apparently the position for which the greatest shift from the all-trans wavenumber occurs, the change is from 1139 to 1140 cm^{-1}. Thus, a chain of the length with which we are concerned, with one gauche bond, has a TO mode of essentially the same wavenumber as an all-trans chain. (2) The relative motion of CH_2 groups along the chain in the TO mode changes phase by about π across the gauche bond. The bond around which the conformer rotation occurs does not change its length during the vibration. Figure 2 shows the approximate motion of the CH_2 groups derived from Snyder's normal modes for $M = 8$, with a single gauche bond, together with the associated normal coordinates. It is to be noted in these cases that the motion looks like that of two all-trans chains with a phase difference of π.

In our lipid bilayer model we explicitly include chain states with up to three gauche bonds and implicitly include all others in the highly excited melted state. Emboldened by Snyder's results that the presence of a single gauche bond has very little effect upon the wavenumbers of the TO mode of $CH_3(CH_2)_{M-2}CH_3$, $M \geq 6$, we shall assume that, because we deal with long chains ($M \geq 14$), the wavenumbers of the TO modes for such chains with up to at least three gauche bonds excited are unchanged from that of the all-trans conformation. The basis for this is that an all-trans segment appears, from Snyder's calculation, to forget within a distance of one C–C bond that it is bounded by a gauche bond. A possible exception might be the case wherein two gauche excitations occupy successive bonds, but there are relatively few such conformations. Furthermore, we shall assume that there is a phase change of π in the normal coordinates across each gauche bond. In Figure 3 we show some assumed normal coordinates of a few chain states together with the motion of the CH_2 groups.

In order to calculate the Raman intensity, we must assign values to the normal coordinates. In Figure 4I we show the local coordinate system which we use, where it is seen that CH_2 groups to the left of the chain axis have a right-handed system while those to the right have a left-handed system. The coordinates of the qth CH_2 group for the mode Q are $\bar{x}_q(Q)$, $\bar{y}_q(Q)$, and $\bar{z}_q(Q)$. Note that the local $\bar{y}$ axes bisect the H–C–H angle and lie in the CH_2 plane. Local axes for a chain with one gauche bond are shown dashed in Figure 4II. For the TO mode of interest, the 1130-cm^{-1} mode, we shall assume for simplicity that all the $\bar{y}_q$ are equal in magnitude, independent of chain configuration. This is true sufficiently far from a gauche bond or from the ends of the chain. We shall assume

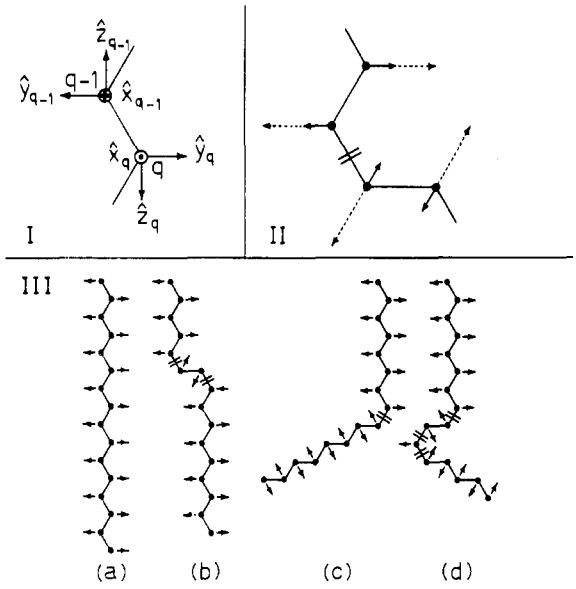

FIGURE 4: (I) The coordinate system used for successive CH_2 groups in a hydrocarbon chain. $\hat{x}_q$, $\hat{y}_q$, and $\hat{z}_q$ are orthonormal vectors for the qth CH_2 group; $\hat{y}_q$ lies in the H–C–H plane and bisects the H–C–H angle. (II) CH_2 motions associated with the TO mode, with the local $\hat{y}$ axes drawn as dashed lines. This enables the sign of the $\bar{y}_q(Q)$ to be deduced for use in eq 7. (III) Relative Raman intensities at 1130 cm^{-1} for a C-16 chain in its TO mode: (a) 256; (b) kink, 144; (c) 0 [(c) is not an intermediate state]; (d) 4. The gauche bonds are indicated by double slashes.

also that the mode is a pure in-plane TO mode so that all $\bar{x}_q$ and $\bar{z}_q$ are zero. The $\bar{z}_q$'s are motions associated with the 1064-cm^{-1} mode, i.e., motion along the local axis of the chain, while the $\bar{x}_q$'s are motions out of the plane of the chain. Neither of these were found to be significant in the analyses [e.g., Snyder (1967)]. Because of the way in which the normal coordinates enter the expression for the intensity, we will see that the contributions from CH_2 groups adjacent to a gauche bond cancel so that a wrong estimate of their contributions is unimportant. This is because there is local reflection symmetry through the center of a gauche bond. The most important excited chain conformers (single gauche states and kinks) all possess this property. Wrong estimates of $\bar{y}_q$ near the ends of the chain are common to nearly all conformers, and, since we calculate only relative intensities, then the errors arising therefrom are small. We feel, therefore, that it is unnecessary to undertake a normal mode calculation for the intermediate states in order to obtain the exact normal coordinates for a few CH_2 groups. In Figure 4II we have shown our CH_2 displacements as solid lines, and we see that as one passes over a gauche bond the signs of the $\bar{y}_q$, for this TO mode, change. This will enable us to calculate relative intensities quite simply.

Finally, we must calculate the Raman scattering intensity of a particular conformation relative to that of the all-trans state. Theimer (1957) calculated the Raman scattering intensity of an all-trans chain in the dipole approximation within a classical framework. He showed that the intensity, $I(Q)$, of a normal mode Q for randomly oriented scatterers is

$$I(Q) \propto \frac{[\nu_0 - \nu(Q)]^4}{\nu(Q)[1 - \exp[-\beta h\nu(Q)]]}[45\alpha'(Q)^2 + 13\gamma'(Q)^2] \tag{4}$$

$$\alpha'(Q)^2 = A^2[\sum_q \bar{y}_q(Q)]^2$$

$$\gamma'(Q)^2 = C^2[\sum_q \bar{x}_q(Q)]^2 + B^2[\sum_q \bar{y}_q(Q)]^2 + D^2[\sum_q \bar{z}_q(Q)]^2$$

$$\beta = 1/k_B T$$

where A, B, C, and D depend upon the derivatives of the polarizability tensor, $\nu(Q)$ is the frequency of the mode Q, and ν_0 is the frequency of the exciting radiation. We assume that the polarizability derivatives are independent of bond position and chain conformation. This will be true far enough away from a gauche bond or from the ends of the chain. Again, errors near the ends of the chain will be common to all conformations. General expressions are given by Snyder (1970) for intensities, but, with our assumption, Theimer's simple expression can be used for our relatively crude calculation.

We thus arrive at two simple rules for calculating intensities for contributions to the 1130-cm^{-1} TO mode: all $\bar{x}_q = \bar{z}_q = 0$. Across a gauche bond the $\bar{y}_q$'s change sign, and all $\bar{y}_q$'s are approximately equal in magnitude. Examples of relative intensities for DPPC are given in Figure 4III.

Finally, we must estimate the intensity of the melted highly excited state. We calculated the average intensities for all conformations, which do not double back toward the head group, with a given number of gauche bonds. We plotted these as functions of their internal energy from 0 to $4E_g$ and extrapolated the curve to the energy of the melted state obtained already. We thus estimated the intensity contributed to scattering by the melted state to be 10 (DMPC, $M = 14$), 15 (DPPC, $M = 16$), and 20 (DSPC, $M = 18$) relative to the respective all-trans intensities of 196, 256, and 324. Changing these numbers by up to 50% produces no significant change in the calculated intensities. The last column of Table I lists the relative Raman intensities for all the states considered.

The denominator $[1 - \exp[\beta h\nu(Q)]]$ need not be considered explicitly because the experimental intensities are plotted as ratios of the 1130-cm^{-1} intensity to that of the 718-cm^{-1} mode. The ratio of the exponential functions for these two lines changes by approximately 1.8% between 120 and 370 K, and so our intensity plots do not include these factors.

In order to calculate thermodynamic quantities, we used a mean field approximation by defining a Hamiltonian

$$H_0 = \frac{-J_0^M}{2}\sum_i\sum_n \lambda_n L_{ni} \tag{5}$$

The free energy is given in the usual way by

$$F = F_0 + \langle H - H_0\rangle_0 \qquad F_0 = -\frac{1}{\beta}\ln Z_0$$

$$Z_0 = Tre^{-\beta H_0} \qquad \langle Q\rangle_0 = Tre^{-\beta H_0}Q/Z_0 \tag{6}$$

where Q is any combination of the projection operators, and the λ_n's are chosen so as to minimize F with respect to them. The main (first-order) phase transition occurs at the temperature where the free energies of the gel and fluid phase are equal. The calculated intensity of the 1130-cm^{-1} line relative to its intensity at sufficiently low temperatures is then

$$I_{1130}(T) = \langle[\sum_q \bar{y}_q(1130)]^2\rangle_0/I_0 \tag{7}$$

where the exponential denominator has been omitted and I_0 is the all-trans intensity.

Experimental Section

L-β,γ-Dipalmitoyl-α-phosphatidylcholine, produced by Fluka (puriss. grade), was obtained from Fluorochem Ltd., Glossop, Derbyshire, and was used without further purification.

Coarse aqueous dispersions of DPPC were obtained by combining dry DPPC with three parts by weight of doubly distilled water in 3.5-mm diameter sample tubes. Vortex

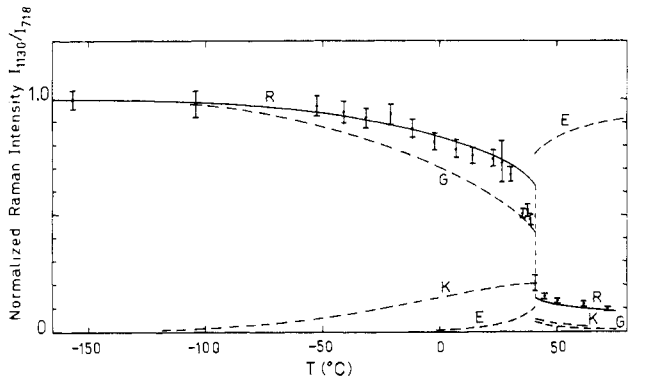

FIGURE 5: Values of the normalized Raman intensity I_{1130}/I_{718} for DPPC bilayers, as a function of temperature. Points with error bars are the measured values and the solid line (R) is the curve calculated as described. Also shown as dashed lines are the probabilities for a hydrocarbon chain to be in its all-trans state (G), any kink state (K), or its excited melted state (E).

mixing, performed above the lipid gel–liquid-crystal transition temperature, yielded homogeneous dispersions, which were then allowed to equilibrate. The dispersions were compacted by light centrifugation before use.

Raman spectra were recorded on a Spex Ramalog 5 instrument having a DPC-2 photon detector; a CRL-52 krypton-ion laser was used for 530.9-nm excitation. The laser power, measured at the sample position, was maintained constant throughout the work at approximately 200 mW. The spectral recording parameters were as follows: slit widths, 400 μm; scanning speed, 0.25 cm^{-1} s^{-1}; photon counting integration time, 2 s; smoothing time constant, 7 s.

Sample temperatures were controlled by using a nitrogen (air) gas flow system for measurements below (above) room temperature in conjunction with a Spex quartz sample cavity. Temperatures were measured by means of a thermocouple within the cavity. A correction for laser heating of the sample has not been made.

The intensities of the 1130-cm^{-1} line were measured with respect to the 718-cm^{-1} line which has been assigned to a C–N stretching mode and which is temperature invariant (Gaber & Peticolas, 1977; Gaber et al., 1978a).

Intensities were measured as peak areas—the areas were obtained by weighing paper cutouts of the peaks. Where necessary, the 1130-cm^{-1} line was decomposed from its broader neighbor (centered on ~1100 cm^{-1}) by eye, and the average of two alternative interpretations of its area was recorded. Each Raman intensity presented is the average intensity ratio (I_{1130}/I_{718}) from four spectra, normalized by the average intensity ratio measured at the lowest temperature (1.64 ± 0.07 at −157 °C). Error bars represent the estimated standard error in the mean result.

Results and Discussion

For DPPC bilayers (M = 16), the results of the calculation of the normalized Raman intensity of the 1130-cm^{-1} line as a function of temperature are shown in Figure 5, together with the experimental data. The agreement between theory and experiment is satisfactory over the whole temperature range considered: the theoretical curve reproduces the observed gradual fall in normalized Raman intensity from 1.0 to approximately 0.7 over the temperature range −100 to 30 °C and above T_c reproduces the total intensity of the fluid hydrocarbon chains. Calculations of the normalized Raman intensity as a function of temperature for DMPC bilayers (M = 14) and DSPC bilayers (M = 18) are shown in Figure 6, together with

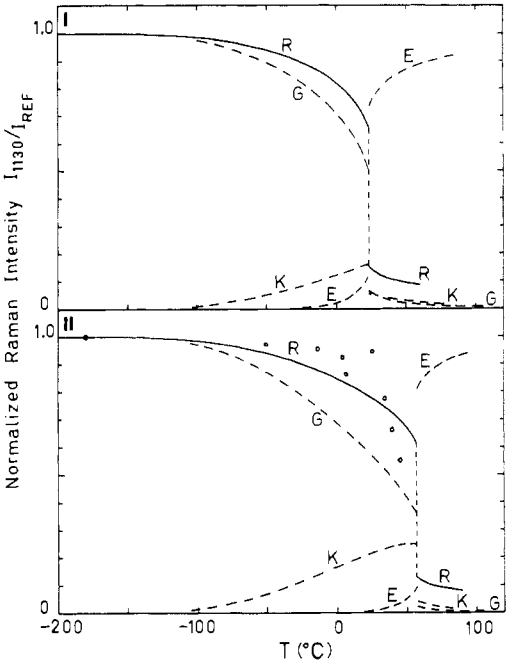

FIGURE 6: Calculated normalized Raman intensities for (I) DMPC bilayers and (II) DSPC bilayers, as a function of temperature, shown as solid lines labeled R. The dashed lines show the probabilities for a hydrocarbon chain to be in its all-trans state (G), any kink state (K), or its excited melted state (E). Also shown in (II) are values of I_{1130}/I_{1295} measured by Yellin & Levin (1977c) and replotted (excluding one point) from their Figure 2.

normalized values of I_{1130}/I_{1295} measured by Yellin & Levin (1977c).

The occurrence probabilities of some of the more probable chain conformations as a function of temperature are also shown in Figures 5 and 6: the all-trans state (labeled G), the single kink state (one $g^{\pm},t,g^{\mp}$ sequence at any chain position, labeled K), and the excited or melted state (corresponding to an average of five gauche bonds per chain in DPPC, labeled E). These probabilities are given by $\langle L_G \rangle_0$, $\langle L_4 \rangle_0$, and $\langle L_E \rangle_0$, respectively.

Referring to Figure 5, at a sufficiently low temperature the hydrocarbon chains in a pure lipid bilayer are in their lowest internal energy state, i.e., the all-trans conformation, and $\langle L_G \rangle_0 = 1$. As the temperature of the bilayer is increased, a fraction of the chains assumes the first excited state of internal energy E_g by incorporating a single gauche rotation. Due to interchain steric restrictions imposed by the bilayer packing, such rotations are most likely to occur at the methyl end of the chain (Marsh, 1974). This first type of chain disorder is moderately probable: the occurrence probability gradually rises to approximately 0.1 at the transition temperature, 40.9 °C. Thus, it is to be expected that, given the experimental signal/noise ratio, the onset of chain disorder in the form of this first excited state would not be detectable by the Raman experiment.

As the temperature increases further, the second excited states of internal energy $2E_g$ start to appear. These are dominated by the single kink states which pack favorably with neighboring chains. It can be seen that $\langle L_4 \rangle_0$ increases to a maximum at the transition temperature, and below this temperature the single kink is the most probable excited state at any temperature above approximately −100 °C. In Figure 5 it is seen that the experimental data indicate an onset of disorder in the bilayers at approximately −50 °C, in approximate agreement with the work of Yellin & Levin (1977c). At this temperature $\langle L_4 \rangle_0$ is sufficiently large to cause an observable decrease in the Raman intensity despite the ex-

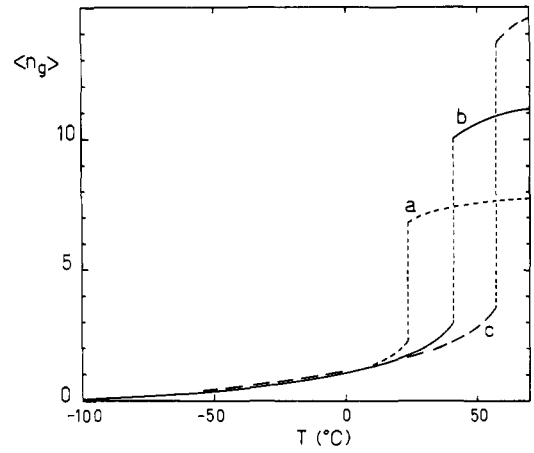

FIGURE 7: Calculated average number of gauche bonds per phosphatidylcholine molecule, $\langle n_g \rangle$, as a function of temperature: (a) DMPC bilayers [$T_c(14)$ = 23.3 °C]; (b) DPPC bilayers [$T_c(16)$ = 40.9 °C]; (c) DSPC bilayers [$T_c(18)$ = 57.0 °C].

perimental signal/noise ratio. The excited or melted state, of low intrinsic Raman intensity, becomes significant at approximately 15 °C.

As the number of chains in excited states increases as the bilayer temperature is raised, the fraction of chains in the all-trans conformation, $\langle L_G \rangle_0$, decreases as seen in Figure 5. The intensity of the 1130-cm^{-1} Raman line has previously been taken by Marsh (1974) as being proportional to the number of all-trans hydrocarbon chains in the bilayer, in which case the normalized Raman intensity would simply be equal to $\langle L_G \rangle_0$. Although $\langle L_G \rangle_0$ as a function of temperature does not deviate greatly from the experimental intensities below T_c, above T_c $\langle L_G \rangle_0$ is approximately a factor of 10 too low to account for the experimental intensities. This is evidence that other chain conformations also contribute to the intensity of the 1130-cm^{-1} line, especially above T_c.

The expression proposed by Gaber & Peticolas (1977) for the intensity of the 1130-cm^{-1} line incorporates the assumption that each trans C–C bond of a chain (in a sequence of at least three) scatters radiation incoherently with any other trans C–C bond of that chain. Our intensity expression, eq 7, which follows from that of Theimer (1957), reflects the coherent nature of the vibration of the entire chain.

Gaber & Peticolas (1977) defined a "trans" order parameter essentially equivalent to the normalized Raman intensities presented here, except that peak heights rather than peak areas were taken to represent line intensities. Because there is no simple relationship between the number of trans bonds in a chain and its relative Raman intensity at 1130 cm^{-1} (as shown by application of eq 7), we feel that such an order parameter can only provide qualitative information concerning the fluidity of the hydrocarbon chains. It is probably unreliable to estimate accurate enthalpy differences between rotational isomers by using this line, as has been done (Yellin & Levin, 1977a,b), since I_{1130} is not linearly proportional to $\langle L_G \rangle_0$. This is demonstrated in the calculation of the average number of gauche bonds per molecule (Yellin & Levin, 1977a), where equating the integrated van't Hoff expression with ln (I_{1090}/I_{1130}) yields the numbers ~2, ~2, and ~6 for DMPC, DPPC, and DSPC, respectively, at temperatures below the respective pretransition temperatures. From Figure 7 we see that the calculated average number of gauche bonds per molecule, $\langle n_g \rangle$, below the pretransition temperatures and above the main transition temperatures is as follows: DMPC, 1.06 (0 °C) and 7.14 (30 °C); DPPC, 1.78 (25 °C) and 10.35 (45 °C); DSPC, 2.22 (40 °C) and 13.98 (60 °C). The value of $\langle n_g \rangle$ for DPPC bilayers above T_c is in agreement with previous estimates (Schindler & Seelig, 1975; Seelig & Seelig, 1974; Nagle, 1973b).

An inflection at approximately 35 °C is apparent in the data in Figure 5. We attribute this to the pretransition or premelting event previously observed in Raman spectra (Gaber & Peticolas, 1977; Yellin & Levin, 1977b; Gaber et al., 1978a). Our theoretical model has no provision for a pretransition mechanism and thus does not account for its effect on the observed Raman intensity.

In conclusion, in addition to other successful applications (Caillé et al., 1980; Pink & Chapman, 1979), the model for the conformer dynamics of a saturated hydrocarbon chain in a lipid bilayer is able to account successfully for the Raman intensity at 1130 cm^{-1} as a function of temperature for the DPPC coarse aqueous dispersion and thus provides a convincing characterization of the hydrocarbon chain ordering in this model biomembrane system. This characterization is a prerequisite for a similar Raman spectroscopic study involving the addition of membrane components such as cholesterol or proteins to this system. Using the approach taken in this paper, with an extension of the dynamical model, we will examine the cholesterol–DPPC–H_2O system in a future publication.

Acknowledgments

D.A.P. thanks Professor H. Stieve for the hospitality of the Institut für Neurobiologie der Kernforschungsanlage where the theoretical work was done and the Alexander von Humboldt-Stiftung for a Forschungstipendiat. DAP also thanks Professor P. Fulde for the hospitality of the Max-Planck-Institut, Stuttgart, and for making computing facilities available there and Professor M. Cardona for a discussion on Raman intensities. Brigitte Rainer (KFA) helped with some computing. T.J.G. and D.C. thank Professor G. Wilkinson for the use of the Imperial College (University of London) Raman spectroscopy facilities and B. P. O'Hare for technical assistance. A reviewer is thanked for drawing our attention to some omissions in the presentation of the theory.

References

Caillé, A., Pink, D. A., de Verteuil, F., & Zuckermann, M. J. (1980) *Can. J. Phys.* (in press).

Chapman, D., Williams, R. M., & Ladbrooke, B. D. (1967) *Chem. Phys. Lipids 1*, 445–475.

Chapman, D., Cornell, B. A., Eliasz, A. W., & Perry, A. (1977) *J. Mol. Biol. 113*, 517–538.

Chapman, D., Gômez-Fernández, J. C., & Goni, F. M. (1979) *FEBS Lett. 98*, 211–223.

Curatolo, W., Verma, S. P., Sakura, J. D., Small, D. M., Shipley, G. G., & Wallach, D. F. H. (1978) *Biochemistry 17*, 1802–1807.

Estep, T. N., Mountcastle, D. B., Biltonen, R. I., & Thompson, T. E. (1978) *Biochemistry 17*, 1984–1989.

Flory, P. J. (1969) *Statistical Mechanics of Long Chain Molecules*, Interscience, New York.

Gaber, B. P., & Peticolas, W. L. (1977) *Biochim. Biophys. Acta 465*, 260–274.

Gaber, B. P., Yager, P., & Peticolas, W. L. (1978a) *Biophys. J. 21*, 161–176.

Gaber, B. P., Yager, P., & Peticolas, W. L. (1978b) *Biophys. J. 22*, 191–207.

Lin, T. P., & Koenig, J. L. (1962) *J. Mol. Spectrosc. 9*, 228–243.

Lippert, J. L., & Peticolas, W. L. (1971) *Proc. Natl. Acad. Sci. U.S.A. 68*, 1572–1576.

Marcelja, S. (1974) *Biochim. Biophys. Acta 367*, 165-174.
Marsh, D. (1974) *J. Membr. Biol. 18*, 145-162.
Nagle, J. F. (1973a) *Proc. Natl. Acad. Sci. U.S.A. 70*, 3443-3444.
Nagle, J. F. (1973b) *J. Chem. Phys. 58*, 252-264.
Pink, D. A., & Carroll, C. E. (1978) *Phys. Lett. A 66*, 157-160.
Pink, D. A., & Chapman, D. (1979) *Proc. Natl. Acad. Sci. U.S.A. 76*, 1542-1546.
Salem, L. (1962) *J. Chem. Phys. 37*, 2100-2113.
Schindler, H., & Seelig, J. (1975) *Biochemistry 14*, 2283-2287.
Seelig, A., & Seelig, J. (1974) *Biochemistry 13*, 4839-4845.
Snyder, R. G. (1967) *J. Chem. Phys. 47*, 1316-1360.
Snyder, R. G. (1970) *J. Mol. Spectrosc. 36*, 222-231.
Snyder, R. G., & Schachtschneider, J. H. (1963) *Spectrochim. Acta 19*, 85-116.
Spiker, R. C., & Levin, I. W. (1975) *Biochim. Biophys. Acta 388*, 361-373.
Tardieu, A., Luzzati, V., & Reman, F. C. (1973) *J. Mol. Biol. 75*, 711-733.
Tasumi, M., Shimanouchi, T., & Miyazawa, T. (1962) *J. Mol. Spectrosc. 9*, 261-287.
Theimer, O. H. (1957) *J. Chem. Phys. 27*, 408-416.
Wulf, A. (1977) *J. Chem. Phys. 67*, 2254-2266.
Yellin, N., & Levin, I. W. (1977a) *Biochemistry 16*, 642-647.
Yellin, N., & Levin, I. W. (1977b) *Biochim. Biophys. Acta 468*, 490-494.
Yellin, N., & Levin, I. W. (1977c) *Biochim. Biophys. Acta 489*, 177-190.

Isolation, Physicochemical Properties, and Macromolecular Composition of Zona Pellucida from Porcine Oocytes†

Bonnie S. Dunbar,‡ Nate J. Wardrip, and Jerry L. Hedrick*

ABSTRACT: Oocytes released en masse from pig ovaries were isolated in large quantities by using sieving techniques. The isolated ooctyes were gently homogenized, and the largely intact zona pellucida "ghosts" were purified by using sieving techniques. Sufficient amounts of zonae were recovered to permit, for the first time, adequate characterization of the zona pellucida in chemical, physical, and macromolecular terms. The isolated zonae were >93% pure as determined by chemical, enzymatic, and microscopic criteria. The zonae were completely solubilized by a variety of conditions that do not break covalent bonds. The extent of solubilization was a function of pH, ionic strength, temperature, and the presence of various solubilizing agents such as detergents and urea. Chemically, the zonae were composed predominantly of protein (71%) and carbohydrate (19%). After acid hydrolysis of the zonae, no unusual amounts or types of amino acids were detected. The monosaccharides present after hydrolysis were those typically found in animal glycoproteins (Fuc, Man, Gal, GalNAc, and GlcNAc). Sialic acid in glycosidic linkage and sulfate and phosphate esters were present and were considered to be true constituents of the zona pellucida. Other substances detected, but considered contaminants rather than true constituents, included fatty acids (esterified and free) and uronic acids. The binding by several fluorescein-conjugated plant lectins to the in situ zona pellucida was determined by using light microscopy. The binding of the lectins to the zona pellucida was not uniform, indicating that the carbohydrate moieties of the zona pellucida were asymmetrically distributed. The zona pellucida was composed of at least three macromolecules as indicated by immunodiffusion and sodium dodecyl sulfate gel electrophoresis experiments. Determination of the number of macromolecules composing the zona pellucida was compromised by the aggregation and/or microheterogeneity of its constituent macromolecules. We conclude that the zona pellucida is composed of several glycoprotein macromolecules; interaction of these macromolecules to form supramolecular complexes and the integral zona pellucida is dependent on noncovalent forces.

The chemical and physical properties of the zona pellucida, the extracellular envelope surrounding mammalian oocytes and eggs adjacent to the plasma membrane, are of particular interest because of its biological importance. In the fertilization process, sperm penetration through the zona pellucida has been postulated to involve a preliminary sperm binding to the zona pellucida [Hartman et al., 1972; Hartman & Hutchison, 1976; for a discussion, see Gwatkin (1977)]. This is followed by a restricted hydrolysis of the zona pellucida with the assistance of sperm enzymes such as acrosin, thereby permitting the sperm access to the egg plasma membrane [Srivastava et al., 1965; Stambaugh & Buckley, 1969; Polakowski et al., 1972; Schleuning et al., 1973; for a discussion, see McRorie & Williams (1974) and Hartree (1977)]. After the fertilizing sperm has gained access to the egg and triggered the cortical reaction, the zona pellucida is chemically and physically modified to prevent supenumerary sperm penetration (Austin & Braden, 1956; Barros & Yanagimachi, 1971, 1972; Gwatkin et al., 1973). In addition to the above, the zona pellucida is currently of intense interest in terms of its immunological properties, as antibodies directed against zona pellucida components prevent sperm binding to the zona pellucida and fertilization of eggs both in vitro and in vivo (Shivers et al., 1972; Ownby & Shivers, 1972; Garavagno et al., 1974; Glass & Hanson, 1974; Jilek & Pavlok, 1975; Oikawa & Yanagimachi, 1975; Tsunoda & Chang, 1976a,b; Yanagimachi et al., 1976; Gwatkin & Williams, 1978).

† From the Department of Biochemistry and Biophysics, University of California, Davis, California 95616. *Received July 16, 1979.* This work was supported in part by a U.S. Public Health Service Grant (HD 04906) to J.L.H. Preliminary reports of some aspects of this work have appeared (Dunbar et al., 1978a,b).

‡ Present address: The Population Council, Center for Biomedical Research, Rockefeller University, New York, NY 10021.

0006-2960/80/0419-0356$01.00/0